

# Numerical simulation of large-scale magnetic-field evolution in spiral galaxies

K. Otmianowska-Mazur<sup>1,2</sup> and M. Chiba<sup>2,3</sup>

<sup>1</sup> Astronomical Observatory, Jagiellonian University, ul. Orla 171, Krakow, Poland

<sup>2</sup> Max-Planck-Institut für Radioastronomie, Auf dem Hügel 69, D-53121 Bonn, Germany

<sup>3</sup> Astronomical Institute, Tohoku University, Sendai 980-77, Japan

Received date 4 August 1994; accepted date 11 February 1995

**Abstract.** The evolution of large-scale magnetic fields in disk galaxies is investigated numerically. The gasdynamical simulations in a disk perturbed by spiral or bar potential are incorporated into the kinematic calculations of induction equations to elucidate the effects of non-axisymmetric disk structure on magnetic fields. The effects of interstellar turbulence are given as the turbulent diffusion of magnetic fields. The usually adopted dynamo mechanism of  $\alpha$ -effect is not considered in our computations, because it is not obvious about the actual existence of the effect in a galaxy. Our principal concern is to clear how *observationally* and *theoretically well-established* gas flow affects the magnetic-field structure and evolution, without putting a lot of artificial parameters in the model.

We have found that the density-wave streaming motion of gas has a significant influence on the distribution of magnetic fields: the lines of force are well aligned with spiral arms due to the compressional and additional shearing flow of gas in these regions. In the inter-arm regions, the field lines have the finite angles with respect to the imposed arms, because the gaseous streamlines induced by spiral arms deviate from the orientation of spiral arms themselves. These properties of magnetic-field orientation across the arm are well in agreement with the results of radio continuum observations. All simulation models have resulted in the eventual decay of magnetic energy due to the strong turbulent diffusion.

We have also explored the azimuthally periodic function for the coefficient of turbulent diffusion with the maximum in spiral-arm regions. This is anticipated from the enhancement of turbulence by young OB stars and supernovae. This effect of non-uniform dissipation gives rise to the modulation of magnetic-field structure and its time evolution. In particular, the dissipation rate of magnetic fields can be much smaller than the usually assumed rate of  $\sim 1/10^8 \text{ yr}^{-1}$ .

Send offprint requests to: K. Otmianowska-Mazur (Krakow),  
e-mail: otmian@oa.uj.edu.pl

**Key words:** magnetic fields - MHD - galaxies: magnetic fields - kinematics and dynamics - spiral

## 1. Introduction

Measurements of linear polarization in radio continuum observations have revealed characteristic morphology of magnetic field configuration in galaxies (Beck 1993): lines of force are well aligned with characteristic features of a disk galaxy such as spiral arms and bars, and a few but not all edge-on galaxies prevail largely vertical fields perpendicular to a disk. Attempts to derive actual directions of magnetic vectors are rather delicate tasks with a lot of ambiguities, and thus have not well succeeded to uncover whether field directions change along the azimuth or not in a galactic disk. The recent high-resolution measurements also allow to derive the fine structure of the large-scale magnetic fields in a disk: pitch angles of these fields vary with azimuthal angle in the systematic way (e.g. Ehle & Beck 1993), and the well uniform fields are most recognizable outside the optical spiral arms. Apparently, these observations suggest that origin of magnetic morphology is principally associated with a non-axisymmetric galactic structure accompanying a characteristic large-scale gas flow.

It has been argued that present structure and typical strength of galactic magnetic fields are organized by induction processes called galactic  $\alpha\omega$ -dynamoes (Krause et al. 1993). Galactic dynamoes are invoked by the self-amplification of magnetic fields via helical small-scale turbulence ( $\alpha$ -effects) and differential galactic rotation ( $\omega$ -effects). Generally initial (seed) magnetic fields are composed of several magnetic modes, and the modes with finite exponential growth are supposed to predominate at the present epoch after some nonlinear saturation of growth. The conventional models are characterized by a

rather slow time scale of field amplification, of the order of Gyr, and attempts have been made to explain the present field structure, mainly based on an axisymmetric disk model with some additional effects of vertical flow. An implicit assumption in such an approach is that a galactic structure is only the second order effect on a magnetic-field structure, and dynamo experts tend to invoke the properties of turbulence (such as tensor  $\alpha$ ) to explain non-axisymmetric magnetic fields (e.g. Rüdiger et al. 1993).

Basically an induction equation says that the magnetic-field evolution is strongly governed by the profiles of velocity fields, which are typically having a time scale for change, of the order of  $10^8$  yrs, in a galactic disk. Then it is followed that most of the present field structures reflect the velocity fields of gas which have happened within  $\sim 10^8$  yrs, irrespective of slow  $\alpha\omega$ -dynamo processes. Dynamos might give a solution for global field geometry (e.g. axisymmetric or bisymmetric), which is however not well defined from observations. It has also been claimed that dynamos cannot explain the strong field at high-redshift intergalactic clouds (Wolfe et al. 1992). Therefore, as most observational results suggest as mentioned above, it is *essential* to clarify the role of a galactic structure in understanding the *present* structure of magnetic fields (see Kronberg 1994 and Chiba & Lesch 1994 for more detailed discussion about the present status).

In the present paper, we focus on the evolution of magnetic fields under the influence of non-axisymmetric disturbance, such as spirals and bars, and perform numerical simulations to elucidate how such disturbances affect the evolution and structure of magnetic fields. With the same motivation, Panesar & Nelson (1992) have shown from their simulation that spiral arms strongly modify the field morphology. Since they have performed only one case due to the extensive nature of simulation, we attempt to consider several cases for the parameters of disturbances, particularly concerning the dependence on pitch angles of spiral arms, and spatial profiles of turbulent diffusion for magnetic fields.

The plan of the paper is as follows: Sec.2 is devoted to methods of simulations and model parameters. Results of simulation are explained in Sec.3. Conclusions and discussion, especially the comparison with observations, are given in Sec.4.

## 2. Numerical Methods and Model parameters

### 2.1. Hydrodynamics in a galaxy

In our simulations of magnetic fields in galaxies, it is crucial to obtain the realistic large-scale flow of gas, which is most plausible theoretically and also reminiscent of observed velocity fields of the neutral gas component as well as the warm ionized gas. We adopt the hydro-code of smoothed particle hydrodynamics (SPH), first introduced by Lucy (1977) and Gingold & Monaghan (1977). The

SPH code is based on a particle method, without defining a computational grid. Thus it is fully Lagrangian, and is naturally implemented in three-dimensional calculations. Because of its flexible nature of the scheme, it is widely used for many astrophysical problems (see e.g. Monaghan 1992; Benz 1990; Hernquist & Katz 1989).

#### 2.1.1. Fundamentals in SPH

In SPH, the computation consists of a number of discrete fluid elements, i.e. particles, so that some local averages must be performed using an interpolating kernel  $W(r; h)$ .  $h$  is the smoothing length. Then any mean value of physical quantity, say  $A(\mathbf{r})$  can be defined by

$$\langle A(\mathbf{r}) \rangle = \int A(\mathbf{r}') W(\mathbf{r} - \mathbf{r}'; h) d\mathbf{r}', \quad (1)$$

where the kernel  $W$  is normalized,  $\int W(\mathbf{r}; h) d\mathbf{r} = 1$ . When the values of  $A(\mathbf{r})$  are known only at finite and discrete points, the integral interpolant is replaced by the following equation,

$$\langle A(\mathbf{r}) \rangle = \sum_{j=1}^N m_j \frac{A(\mathbf{r}_j)}{\rho_j} W(\mathbf{r} - \mathbf{r}_j; h), \quad (2)$$

where  $m_j$  is the particle mass; the density  $\rho_j$  at each particle's position is defined as

$$\rho = \sum_{j=1}^N m_j W(\mathbf{r} - \mathbf{r}_j; h). \quad (3)$$

In our simulation, we adopt the kernel based on spline functions (Monaghan & Lattanzio 1985),

$$W(r; h) = \frac{1}{\pi h^3} \begin{cases} 1 - (3/2)x^2 + (3/4)x^3 & \text{for } 0 \leq x \leq 1 \\ (1/4)(2-x)^3 & \text{for } 1 \leq x \leq 2 \\ 0 & \text{for } x \geq 2, \end{cases} \quad (4)$$

where  $x = r/h$ . Here the smoothing length is variable in each particle,  $h_j$ , according to the density at the particle's position (see below).

The hydrodynamical equations in our model are given by

$$\frac{d\mathbf{r}_i}{dt} = \mathbf{v}_i, \quad (5)$$

$$\frac{d\mathbf{v}_i}{dt} = -\frac{1}{\rho_i} \nabla P_i + \mathbf{q}_i - \nabla \Phi - 2\Omega_p \times \mathbf{v} - \Omega_p \times \Omega_p \times \mathbf{r}, \quad (6)$$

$$\frac{dh_i}{dt} = -\frac{h_i}{3\rho_i} \frac{d\rho_i}{dt}, \quad (7)$$

where  $P_i$  is the pressure,  $\Phi$  the gravitational potential, and  $\mathbf{q}_i$  is the artificial viscosity to treat the formation of shock waves. Since our aim is to obtain the characteristic structure of velocity fields in a galaxy, where the effect of self-gravity of gas is minor (except at the galactic center), we neglect the contribution of gas itself in  $\Phi$

but consider the external galactic potential provided by galaxy mass as a whole.  $\Omega_p$  denotes the pattern speed of non-axisymmetric disturbance in a galactic structure (see next section). Therefore we simulate the gas dynamics in a frame rotating with  $\Omega_p$ , where such disturbance is observed to be stationary.

The terms of pressure gradient and artificial viscosity are written as:

$$\frac{\nabla P_i}{\rho_i} + \mathbf{q}_i = - \sum_{j=1}^N m_j \left( \frac{P_j}{\rho_j^2} + \frac{P_i}{\rho_i^2} + \Pi_{ij} \right) \times \frac{1}{2} [\nabla_i W(r_{ij}; h_i) + \nabla_i W(r_{ij}; h_j)], \quad (8)$$

where  $\Pi_{ij}$  denotes the contribution of artificial viscosity given by

$$\Pi_{ij} = \begin{cases} \frac{-\alpha \bar{c}_{ij} \mu_{ij} + \beta \mu_{ij}^2}{\rho_{ij}} f & \text{for } \mathbf{v}_{ij} \cdot \mathbf{r}_{ij} < 0 \\ 0 & \text{for } \mathbf{v}_{ij} \cdot \mathbf{r}_{ij} \geq 0, \end{cases} \quad (9)$$

and

$$\mu_{ij} = \frac{h_{ij} \mathbf{v}_{ij} \cdot \mathbf{r}_{ij}}{\mathbf{r}_{ij}^2 + \eta^2}. \quad (10)$$

Here,  $h_{ij} = (h_i + h_j)/2$ ,  $\bar{\rho}_{ij} = (\rho_i + \rho_j)/2$ , and the average sound velocity,  $\bar{c}_{ij} = (c_i + c_j)/2$ . In the expression for  $\Pi_{ij}$ , eq.(9), the first term corresponds to a bulk viscosity while the second term is equivalent to the Von Neumann-Richtmyer viscosity. For the parameters  $(\alpha, \beta, \eta)$ , we adopt,  $\alpha = 1$ ,  $\beta = 2$ , and  $\eta^2 = 0.01 h_{ij}^2$ , which reproduce reasonably some test calculations such as one-dimensional shock-tube problem and two-dimensional wind-tunnel problem. The factor  $f$  is introduced to prevent the excessive shear viscosity that appears in the standard form of viscosity given in eqs.(9) and (10). In our computation, we use the form for  $f$  described by Benz (1990) as,

$$f = \frac{|\langle \nabla \cdot \mathbf{v} \rangle|}{|\langle \nabla \cdot \mathbf{v} \rangle| + |\langle \nabla \times \mathbf{v} \rangle| + 0.001 \bar{c}_{ij} / h_{ij}}, \quad (11)$$

which vanishes if the quantity  $\langle \nabla \times \mathbf{v} \rangle$ , the curl of velocity is large, suppressing the shear viscosity.

The interstellar gas is modeled in terms of the isothermal equations of state,  $P = c^2 \rho$ .

The basic equations eq.(5), eq.(6), and eq.(7) are integrated in time, using the leapfrog method. The time step  $\Delta t$  is controlled by the Courant condition:

$$\Delta t = 0.3 \min \frac{h_i}{h_i |\nabla \cdot \mathbf{v}| + c_i + 1.2(\alpha c_i + \beta \max_j |\mu_{ij}|)}. \quad (12)$$

### 2.1.2. Galaxy models

The axisymmetric part of the gravitational potential in a disk plane is represented as the Toomre disk (Toomre 1963) :

$$\phi_0(r) = -\frac{c^2}{a} (r^2 + a^2)^{-1/2}, \quad (13)$$

which gives the maximum rotational velocity  $v_{max} = (4/27)^{1/4} c/a$  at a radius  $r_{max} = a\sqrt{2}$ . For the vertical dependence of the potential, we adopt a parabolic form,  $\nu z^2/2$ , where  $\nu$  is the vertical frequency for motions of stars. We use the characteristic value in the solar neighborhood,  $\nu = 3.2 \times 10^{-15} \text{ s}^{-1}$  (Binney & Tremaine 1987), for all radii. Of course, this value as well as the parabolic approximation does not hold all over a disk, especially at high  $z$  where this approximation is invalid. The gas flow derived from this galactic potential is however well representative of actual flow for the present purpose to simulate the magnetic-field evolution.

Initially the gas disk has the approximately uniform density with a finite thickness as determined by the vertical dependence of the potential given above and the sound speed of gas,  $c$ , which is assumed to be constant,  $8 \text{ km s}^{-1}$ . The disk is set up in centrifugal equilibrium. The parameter  $a$  in eq.(13) is  $2.6 \text{ kpc}$  in our simulation, and  $c$  is determined so that  $v_{max} = 200 \text{ km s}^{-1} \text{ kpc}^{-1}$ .

Non-axisymmetric disturbances are introduced to a disk in the first  $1.6 \times 10^8$  yrs of time evolution, with the form,

$$\phi_1(r, \varphi) = \phi_0(r) \varepsilon(r) \cos[2 \ln(r/r_0) \cot \psi + 2\varphi], \quad (14)$$

and are fixed hereafter (Matsuda & Isaka 1980; Johns & Nelson 1986).  $\psi$  is the pitch angle of spiral disturbance with a logarithmic two-armed form, and  $r_0$ , arbitrary parameter, determines the phase of spiral.  $\varepsilon(r)$  is represented as

$$\varepsilon(r) = \varepsilon_0 \frac{r^2}{a^2} \left(1 + \frac{r^2}{a^2}\right)^{-3/2}, \quad (15)$$

which reaches the peak value  $\varepsilon_0 \sqrt{4/27}$  at a radius  $r_{max}$ . In the simulation for a bar perturbation, the term proportional to  $\cot \psi$  in eq.(14) is omitted.

Figure 1 shows the rotation curve and some frequency distribution in our model. It follows that the strength of velocity shear is strongest at  $r \sim 3 \text{ kpc}$ .

In order to obtain the characteristic velocity fields for solving the magnetic-field evolution, the computations of gas dynamics are halted after a few hundreds Myr when the gas flow becomes approximately steady, and then the velocity fields are evaluated as will be explained in the next section. We note that a small-scale time-dependent modulation in gas dynamics is observed (cf. Johns & Nelson 1986), but the obtained velocity profiles by the above procedure are enough characteristic to see their effects on magnetic fields. As an example, the velocity-field vectors for the pitch angle  $20^\circ$  is presented in Fig. 2. The profiles of gas density for the spiral pitch angles,  $10^\circ$  and  $20^\circ$ , and the bar perturbation are shown in Fig. 3. The solid lines mark the minima of the gravitational potential of spirals.

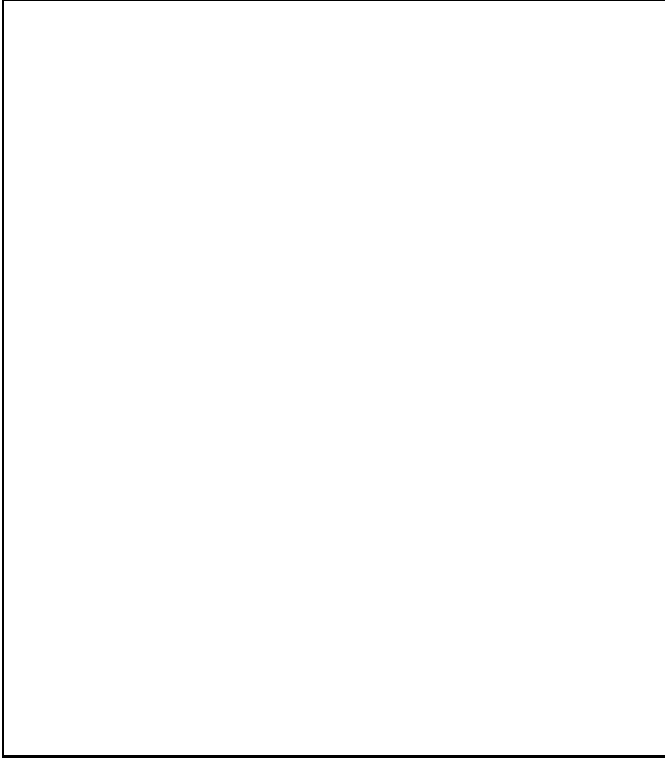


**Fig. 1.** The rotation curve (a) and frequency distribution (b) in the galaxy model

## 2.2. Solving induction equations

The kinematic evolution of the magnetic field is analyzed using the time dependent solution of the field transport equation with diffusion (the induction equation),

$$\partial \mathbf{B} / \partial t = \nabla \times (\mathbf{v} \times \mathbf{B}) - \nabla \times \eta (\nabla \times \mathbf{B}), \quad (16)$$

where  $\eta$  is the diffusion coefficient,  $\mathbf{B}$  and  $\mathbf{v}$  are the magnetic and velocity fields, respectively. The assumed approach allows us to investigate qualitatively the effects of spatially variable  $\eta$  on the evolution of magnetic fields in a disk. However, the more precise solution of this problem is also possible (Kichatinov & Rüdiger 1992).

The problem is solved numerically in three-dimensional (3D) rectangular grid of points, where the  $XY$  plane is the galactic plane and the  $Z$ -axis is the axis of galactic rotation pointing to the North. The rectangular size in  $X$  and  $Y$  directions is 20 kpc, where the grid interval is 400 pc. Along the  $Z$  axis the box has 3 or 4 kpc depending on the assumptions concerning the diffusion coefficient (see below) and with the spatial step of 250 pc interval. The time interval is  $\Delta t = 0.22 \cdot 10^6$  yrs. The fourth order explicit Runge-Kutta method is used for the discretization in time. The space derivatives are approximated by the spline functions of the third order. As the boundary conditions, the continuity of the third order derivatives of the spline functions has been used. Physically it means that impenetrable walls have been applied.



**Fig. 2.** The velocity field vectors in the case of the spiral pitch angle  $\psi = 20^\circ$

This fact causes the necessity of the velocity field decreasing near the edges.

The prevalent number of numerical methods applied to the induction equation do not satisfy the divergence-free condition of the magnetic field. There are several approaches which can be used to solve this difficult problem (Elstner et al. 1990; Evans & Hawley 1988; Schmidt-Voigt 1989). We have adopted the “divergence-cleaning” method elaborated by Schmidt-Voigt (1989) which is suitable in our case (see discussion in Schmidt-Voigt 1989 and Evans & Hawley 1988). Following Schmidt-Voigt, in order to diminish the errors of the non-zero magnetic divergency, we introduce a potential  $\Phi_b$  which is a solution of the Poisson equation,

$$\nabla^2 \Phi_b(x, y, z, t) = -(\nabla \cdot \mathbf{B}). \quad (17)$$

After each time step, this equation is solved using the Gauss-Seidel iteration, and we replace the magnetic field  $\mathbf{B}$  by

$$\mathbf{B}' = \mathbf{B} + \nabla \Phi_b. \quad (18)$$

The iteration ends when the following condition is fulfilled:

$$|(\nabla \cdot \mathbf{B})| \cdot |\Delta x| / |\mathbf{B}| < 0.01. \quad (19)$$

This is what is necessary to avoid the unphysical solutions (Schmidt-Voigt 1987).

To incorporate the particle-based flow in SPH into the grid-based code for magnetic-field evolution described above, the averaging of velocity fields in grids is performed

using the smoothing length  $h_i$  in SPH and Gaussian kernel  $W_g$  (Habe, *et al.* 1991):

$$\mathbf{v}_{ijk} = \frac{1}{\rho_{ijk}} \sum_{n=1}^N m_n \mathbf{v}_n W_g(\Delta r_{ijk,n}; h_n), \quad (20)$$

where  $\Delta r_{ijk,n} = [(x_n - x_i)^2 + (y_n - y_j)^2 + (z_n - z_k)^2]^{1/2}$ ,  $\rho_{ijk} = \sum_n m_n W_g(\Delta r_{ijk,n}; h_n)$ , and  $W_g = 1/\pi^{3/2}/h_n^3 \exp[-(r/h_n)^2]$ . Here the indexes  $i, j, k$  are for grids, and  $n$  for particles. The reason to adopt the Gaussian kernel in this procedure is that due to the finite number of particles ( $N = 2000$ ), there would be the lack of velocities at some grids in the spline case, because  $W$  defined in eq.(4) is zero for  $r/h > 2$ . However, the different choice of kernel for velocity fields at grids does not introduce the fundamental change in the characteristic properties of gas flow obtained in SPH.

The computations have been performed using Cray Y-MP in HLRZ Jülich and SPARC 10 in the Max-Planck-Institut für Radioastronomie in Bonn.

### 2.3. Model parameters

Having combined 3-D SPH code with 3-D induction code, we simulate the evolution of magnetic-field structure and strength in a model spiral galaxy. Although there are many factors to affect velocity-field properties, owing to the limitation of available computation time, we will focus only upon some characteristic gas flows.

The model parameters adopted in the computations are summarized in Table 1. Our models are divided into 2 groups depending on the initial condition for the magnetic field: axisymmetric and uniform field configurations. Though more general would be the superposition of several magnetic modes (Panesar & Nelson 1992), these initial conditions are enough to see the possible effects of non-axisymmetric velocity disturbances, and also the predominant field configurations revealed in radio observations. In Table 1, the models  $A_i (i = 1 - 4)$  are devoted to the initially axisymmetric magnetic-field configuration. Models  $B_i (i = 1 - 7)$  correspond to initially uniform (parallel to the Y axis) magnetic-field structure. The intensity of the field is  $1 \mu G$  in both cases from the reason that the microgauss order of initial magnetic fields after a disk formation has been suggested by the observations of damped Ly $\alpha$  clouds (e.g. Kronberg *et al.* 1992, Wolfe *et al.* 1992), and an idea to explain such observations was given in Lesch and Chiba (1994). Note that since the present concern is devoted to linear processes and the resultant structure of magnetic fields, the actual value of initial field strength does not change our results. The vertical velocity of gas is forced to be zero in all experiments for the sake of simplicity. For the diffusion coefficient  $\eta$ , we adopt the magnitude resulting from the small-scale turbulent gas motions. Its basic value in a galactic plane is  $\eta_0 = 5.7 \cdot 10^{27} \text{ cm}^2 \text{ s}^{-1}$ . This rather high value for  $\eta_0$

**Fig. 3.** The profiles of gas density (grayplot) in the cases of the spiral pitch angle  $\psi = 10^\circ$  (a),  $\psi = 20^\circ$  (b), and the bar (c). The solid lines denote the minima of the gravitational potential of spirals

**Table 1.** The model parameters

Model	$\varepsilon_0$	Pitch angle $\psi$ ( $^\circ$ )	$\Omega_p$ (km/s/kpc)	Corotation (kpc)	$\eta$	$B^{t=0}$ (Inclination $i^\circ$ )	$Z_{max}$	Comments
A1	0.1	10	18	9.1	$\eta(z)$	ring(0)	3	$R_m = 55$
A2	0.1	10	18	9.1	$\eta(r, \varphi, z)$	ring(0)	4	$R_m = 145$
A3	0.1	20	18	9.1	$\eta(z)$	ring(0)	3	$R_m = 55$
A4	0.1	90(bar)	30	6.2	$\eta(z)$	ring(0)	3	$R_m = 55$
B1	0.0	—	—	—	$\eta(z)$	uniform(0)	3	circular rotation, $R_m = 55$
B2	0.1	10	18	9.1	$\eta(z)$	uniform(0)	3	$R_m = 55$
B3	0.1	20	18	9.1	$\eta(z)$	uniform(0)	3	$R_m = 55$
B4	0.1	90(bar)	30	6.2	$\eta(z)$	uniform(0)	3	$R_m = 55$
B5	0.1	10	18	9.1	$\eta(r, \varphi)$	uniform(0)	3	$R_m = 178$
B6	0.1	10	18	9.1	$\eta(r, \varphi, z)$	uniform(0)	4	$R_m = 145$
B7	0.1	10	18	9.1	$\eta(z)$	uniform(0)	4	$R_m = 430$

compared to the usually adopted value is to reduce the computational time for solving the induction equation. We have confirmed from the simulation with smaller  $\eta_0$  that the essential results do not change at all. We note that this order of magnitude for  $\eta_0$  is close to the upper limit of the turbulent diffusion coefficient for the interstellar gas suggested in the literature (Lesch 1993).

We have introduced the  $z$ -dependent diffusion coefficient,  $\eta(z)$ : the presence of the active corona in the galaxy with high temperature ( $10^6$  K) and the high turbulent velocity causes the increase of  $\eta$  in the direction perpendicular to the galactic plane (Camenzind & Lesch 1994; Spencer & Cram 1992). From this reason we have applied the following form for  $\eta$  (Spencer & Cram 1992):

$$\eta = \begin{cases} \eta_0 & \text{for } z \leq H_{\text{dif}} \\ \eta_0 \cdot \exp((z - H_{\text{dif}})/h) & \text{for } H_{\text{dif}} < z \leq H_{\text{max}} \\ \eta_{\text{max}} & \text{for } z > H_{\text{max}}, \end{cases} \quad (21)$$

where  $\eta_0$  is our basic value of the diffusion coefficient,  $H_{\text{dif}}$  ( $= 0.4$  kpc) is the scale height of the interstellar gas, and  $h$  is the scale length of the increase of  $\eta$ . In our case,  $h = 500$  pc, so that  $\eta$  increases about 2.5 times that in the galactic plane. In order to stabilize the code near the boundaries in the vertical direction, the diffusion coefficient above  $H_{\text{max}} = 1$  kpc is constant with a value  $\eta_{\text{max}} \cong 1.4 \cdot 10^{28} \text{ cm}^2 \text{ s}^{-1}$ . The average value of  $\eta$  adopted above suggests a magnetic Reynolds number  $R_m \cong 55$  [defined as  $R_m = v_{\text{max}} L / \eta$ , where  $v_{\text{max}}$  is the maximum value of the velocity field ( $200 \text{ km s}^{-1}$ ), and  $L$  the radius of the model galaxy (10 kpc)]. Relatively high value of  $\eta$  causes the characteristic evolution time of magnetic field less than  $10^9$  yrs, thereby allowing us to reduce the actual time of computation. However, for one experiment, we have adopted the diffusion coefficient ten times smaller than the basic one, for which we have applied  $\Delta t = 10^5$  yrs and assumed the uniform magnetic field as an initial

field configuration. As a result, we obtain  $R_m = 430$  (Table 1, B7).

In order to take into account the influence of spiral-arm activity on the diffusion coefficient, we have adopted the following form for  $\eta(r, \varphi)$ :

$$\eta(r, \varphi) = \frac{\eta_0 - \eta_{\text{min}}}{2} [1 + \cos\{2\varphi + 2 \ln(r/r_0) \cot \psi\}] + \eta_{\text{min}}, \quad (22)$$

where  $\eta_{\text{min}}$ , the minimum value of  $\eta$ , is equal to  $\eta_0/10$  in our model. Equation (22) is equivalent to eq.(14), i.e. we assume the two-armed logarithmic spirals for  $\eta$ . Since the turbulent velocity of interstellar gas,  $\langle v^2 \rangle^{1/2}$ , would be high in arm regions due to efficient energy input from young OB stars and supernovae, the turbulent diffusion,  $\eta \sim \langle v^2 \rangle^{1/2} l$  where  $l$  is the correlation length of turbulence, would be also large (Ko & Parker 1989). Therefore, we assume in our simulations that  $\eta$  is maximum in arm regions. Of course, it is not obvious as to whether this assumption is realistic or not. However, the depolarization of radio continuum emission preferentially in arm regions may support this idea (e.g. Horellou et al. 1993; Neinger et al. 1993). The magnetic Reynolds number is about 178 in this case (B5).

Two experiments (A2 and B6) have been made for the diffusion coefficient variable in the galactic plane as well as in the  $z$  direction accordingly to the above formulae (21 and 22). The averaged value of  $\eta$  gives as a result  $R_m = 145$ .

To avoid numerical instabilities related to the steep diffusion gradients,  $\eta$  has a constant value in the central part of the disk (to the radius of 2 kpc) in all cases.

### 3. Results

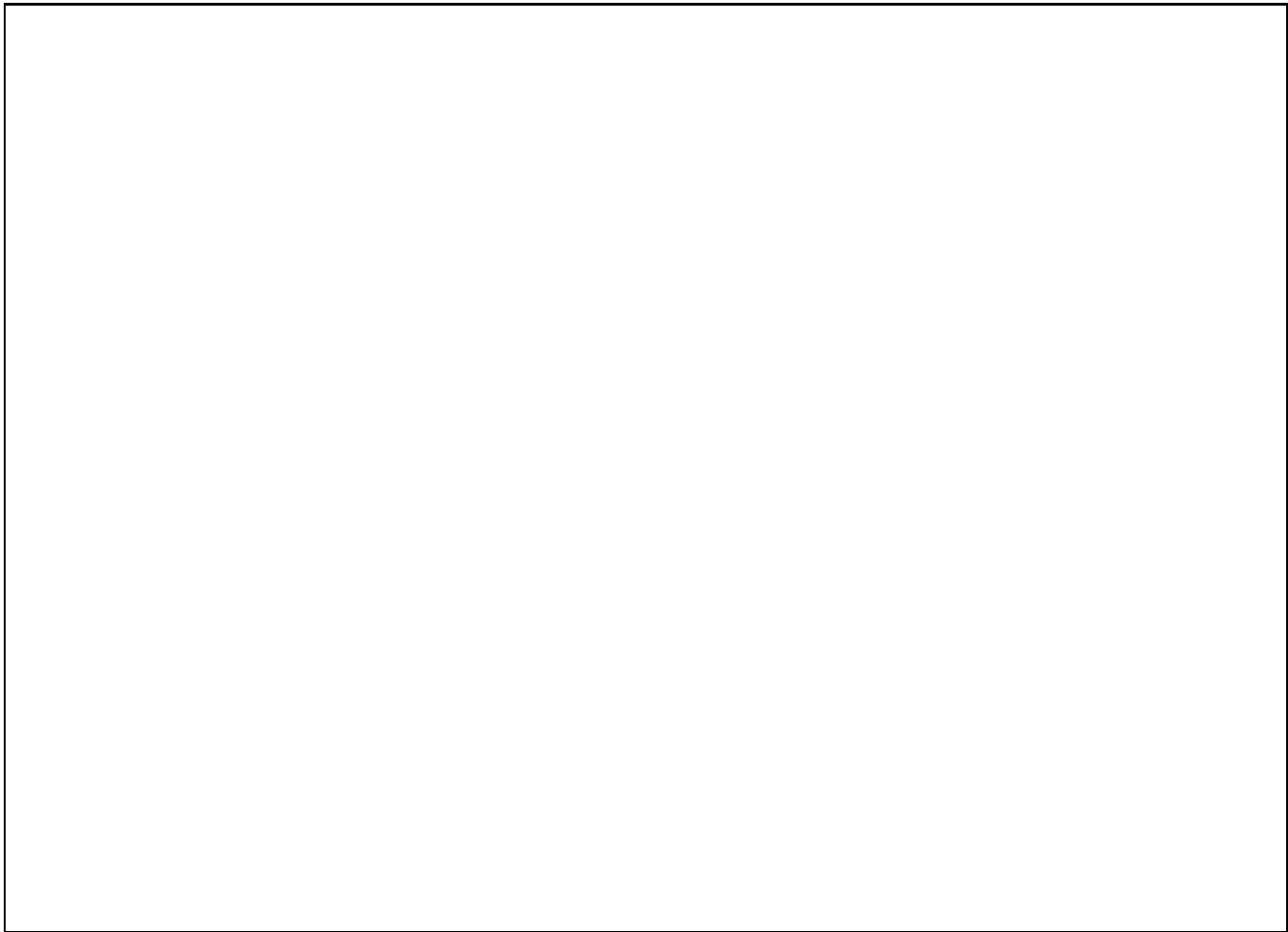


**Fig. 4.** Intensities of magnetic fields (grayplot) and magnetic vectors for the model A1 at  $t = 1.1 \cdot 10^8$  yrs (a) and at  $t = 2.2 \cdot 10^8$  yrs (b), and for the model A2 at the same epochs (c) and (d). The solid lines denote the minima of the gravitational potential of spiral arms

### 3.1. The 3D evolution of magnetic field: the case of initially an axisymmetric magnetic field

The calculations with initially a ring magnetic field structure have been done for three types of gaseous velocity fields (Table 1; A): two-armed spiral disturbances with the pitch angle  $\psi$  being  $10^\circ$  and  $20^\circ$ , and the bar perturbation. By these experiments, we attempt to clarify the net influence of non-axisymmetric disturbance on an axisymmetric magnetic-field distribution. In all cases, the magnetic field follows closely the gas motions, thus prevailing similar structures to spirals or a bar at early evolutionary stages. As time progresses, the field is expelled out from the inner part of the disk due to the adopted strong turbulent diffusion.

Fig. 4 presents the grayplots of the intensity and the vectors of the magnetic field in the galactic plane, for the models A1 with  $\eta(z)$  (a and b), and A2 with  $\eta(r, \phi, z)$  (c and d). Fig. 4a and 4c corresponds to the evolution-

ary stage of  $t = 1.1 \cdot 10^8$  yrs, while Fig. 4b and 4d for  $t = 2.2 \cdot 10^8$  yrs. The solid lines denote the minima of the gravitational potential of spirals. For both experiments, the initially circular field is transformed into the spiral structure (a and c) and then diminishes by the strong diffusion (b and d). The intensity maxima of the magnetic field are visible slightly outside the potential minima (i.e. down-stream side), which are close to the regions where the velocity shear is the highest one. Comparing Fig. 4 with the gas density map for  $\psi = 10^\circ$  (Fig. 3a), it follows that the maxima of the magnetic field coincide with those of gas density, though in the magnetic field case, the outer magnetic layers of the galactic disk are much more dispersed.

Fig. 4 also shows the visible difference between the experiment with the diffusion coefficient  $\eta(z)$  and  $\eta(r, \phi, z)$ : the applied contrast of  $\eta$  between the interarm and arm regions causes higher magnetic field amplification near and inside the spiral arms. It means that the variability of the

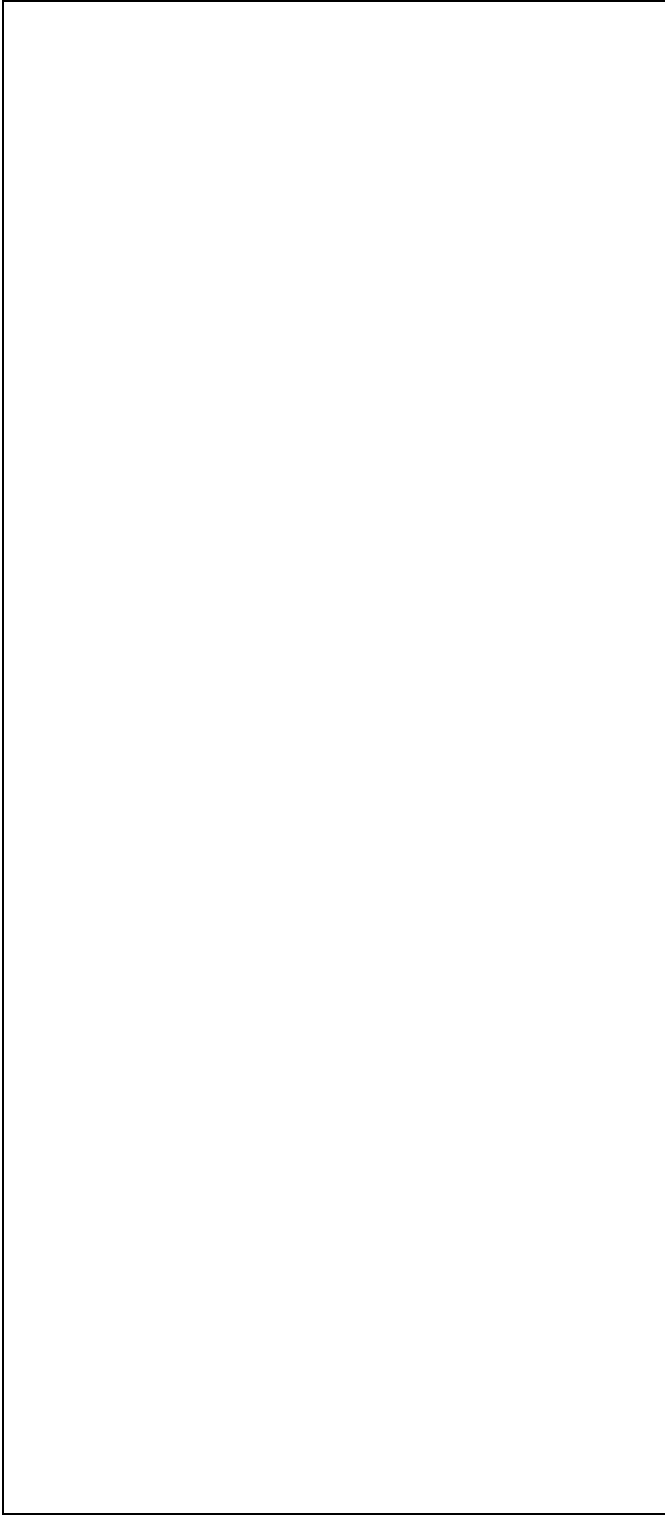


**Fig. 5.** The grayplots of pitch angle distributions of magnetic fields for  $\psi = 10^\circ$ . The dark (white) areas denote the positive (negative) pitch angles (the colors range from  $-25^\circ$  to  $25^\circ$  every  $2^\circ$ ). The solid lines mark the gravitational potential minimum. (a): A1 with  $\eta(z)$ . (b): A2 with  $\eta(r, \varphi, z)$ . Fig.5(c) shows the pitch-angles of velocity fields

diffusion coefficient can play an important role in the evolution of galactic magnetic fields.

One of the most important goals of our simulations is to answer the question how closely the magnetic field follows the interstellar gas motions. In order to analyze it, we introduce the pitch angles of magnetic and velocity fields, defined as the angle between the field vector and the azimuthal direction in the galactic plane. We note that the obtained distribution of magnetic pitch angles is not directly compared with observational results, because the model does not take into account some observational effects such as the beam smoothing or the Faraday rotation. Our aim is to clear the physical connection between magnetic and velocity fields, which is free from ambiguities in interpretation of observations, and tremendous number of freedom in parameters depending on galaxy inclinations, disk thickness, effects of small-scale magnetic fields, and so on.

Fig. 5 shows the grayplots of the magnetic pitch angles at evolutionary time  $t = 1.1 \cdot 10^8$  yrs in the cases of  $\eta(z)$  (A1) (Fig. 5a) and  $\eta(r, \phi, z)$  (A2) (Fig. 5b), as well as, the pitch-angle distribution of the velocity field with  $\psi = 10^\circ$  (Fig. 5c). The dark areas correspond to positive pitch angles - the vectors are directed outward from the disk compared to the azimuthal direction, while the white ones for negative pitch angles - the vectors are directed inward. The absolute maximum values of the modelled pitch angles are below  $30^\circ$  what is in good agreement with observational data (e.g. Neining 1992, Beck 1993). The solid line, as in Fig. 4, shows the minimum of gravitational potential of spirals. It is easily seen that all three maps for pitch angles are very similar: the velocity field as well as the magnetic one is directed outward in front of the potential minimum (i.e. upper-stream side), then is aligned along the spiral arms, and finally is directed inward the galaxy. The highest contrast in the intensities of pitch angle is obtained for  $\eta(r, \phi, z)$ , manifesting the greatest evolutionary changes of magnetic-field structure due to the gas motions and the diffusion.

The numerical experiment using spiral velocity fields with  $\psi = 20^\circ$  (model A3) has resulted in the higher amplification of the magnetic-field intensity (Fig. 6a and 6b, the legend is the same as in Fig. 4a and 4b). The maxima are distributed just outside the potential minimum, more significantly than in the previous case. As obtained for  $\psi = 10^\circ$ , the magnetic maxima coincide with the gas density maxima (see Fig. 3b). Fig. 6a is drawn at  $t = 1.1 \cdot 10^8$  yrs. When we apply two times longer evolution (Fig. 6b), the magnetic flux decreases more slowly than in the A1 or A2 computations. Fig. 6c and 6d present the pitch angle grayplots for the magnetic and velocity fields, respectively. The description is the same as for Fig. 5. The distribution of both fields is almost identical. The magnetic as well as the velocity field are directed outward from the disk in front of the spiral potential, then are tightly aligned with the arms, and finally they point in-





**Fig. 6.** Results of the model *A3*. (a) and (b) show the magnetic-field intensity (grayplot) and vectors at  $t = 1.1 \cdot 10^8$  yrs and  $t = 2.2 \cdot 10^8$  yrs, respectively. (c) and (d) show the pitch-angle distributions of magnetic and velocity fields, respectively. The solid lines denote the gravitational potential minimum

ward. Thus the situation is similar to the  $\psi = 10^\circ$  case, but now, due to the higher non-axisymmetry in the gas flow, the shear is stronger, causing higher magnetic field amplification. However the absolute maximum value is again less than  $30^\circ$ .

The last case for initially a ring magnetic field is the experiment with the bar perturbation on the gaseous velocity field (model *A4*; Fig. 7). The magnetic intensity maxima are not large (Fig. 7a) and they are fully dispersed at the evolutionary stage of  $t = 2.2 \cdot 10^8$  yrs (Fig. 7b). In the central part of the disk, the strong diffusion sweeps the flux quite significantly. The shear in the gas velocity is

not high so that the amplification of magnetic field is low. The distribution of the magnetic pitch angles, which are also similar to those of the velocity fields, proves that the magnetic field is aligned along the bar and arms, changing its direction from outward to inward across the bar and spiral structures.

The magnetic energy density decreases in all cases presented, reaching the lowest value after  $5 \cdot 10^8$  yrs due to the strong turbulent diffusion.

### 3.2. Results for initially a uniform magnetic fields

The calculations of magnetic field evolution with initially a uniform (parallel to the  $Y$  axis) magnetic field have been performed for four velocity field configurations (Table 1; models  $Bi$ ): the pure circular motion with differential rotation, spiral disturbances with  $\psi$  being  $10^\circ$  and  $20^\circ$ , and the bar perturbation.

For all experiments, the magnetic field is wound into the bisymmetric structure, causing the initial growth of the magnetic energy density (Fig. 8). As time progresses, the flux in the inner part of the disk is quickly swept out by the turbulent diffusion, and the magnetic energy decreases. Fig. 8 demonstrates the time evolution of the magnetic energy density  $\epsilon$  normalized to the initial energy density  $\epsilon_0$ . The curves are presented for four chosen cases with Reynolds number  $R_m = 55$  ( $Bi(i = 1 - 4)$ ),  $R_m = 178$  ( $B5$ ),  $R_m = 145$  ( $B6$ ) and the case with  $R_m = 430$  ( $B7$ ). On the contrary to the experiments with initially a ring magnetic field, the smallest growth of  $\epsilon$  occurs for the spiral velocity with  $\psi = 10^\circ$ , while the largest one for the bar disturbance (the cases  $Bi(i = 1 - 4)$ ). It follows that for the flow with higher non-axisymmetry, the winding and dispersing of the magnetic field is faster. The case with  $\eta(r, \phi, z)$  and  $\psi = 10^\circ$  ( $B6$ ) gives the highest increase of the magnetic energy, mainly due to the smaller average value of the diffusion coefficient. The experiment  $B5$  with the diffusion coefficient variable in the galactic plane, but constant in the  $z$  direction (what could have place for galaxies without the active corona) reveals two times bigger growth of  $\epsilon$  and farther maximum with slowly decreasing slope manifesting sustaining of the magnetic field longer than the computation time.

The calculations for the largest Reynolds number of  $R_m = 430$  ( $B7$ ) are the most realistic to the real galaxy conditions. The growth of the magnetic energy density is about three times greater than for the same experiment with  $R_m = 55$  ( $B2$ ). The curve in this case does not decrease smoothly but shows two farther maxima. This fact is well demonstrated in the maps of the magnetic-field vectors shown in Fig. 9. After  $10^8$  yrs, the clear bisymmetric structure is visible with the slightly dispersed in the center (Fig. 9a). This configuration, though more diffusive, can be still observed at  $t = 2 \cdot 10^8$  yrs (Fig. 9b) and  $t = 3.5 \cdot 10^8$  yrs (Fig. 9c). In Fig. 9d, the magnetic flux is completely swept from the central part of the disk, whereas there is still a kind of ring-like field structure in the regions near the edges. It means that for experiments with smaller diffusion coefficient, magnetic field structures will be longer affected by the non-axisymmetric gas flows.

## 4. Conclusions and discussion

The evolution of large-scale magnetic field in the galactic disk affected by non-axisymmetric structures like spirals and bars has been demonstrated using the 3D nu-

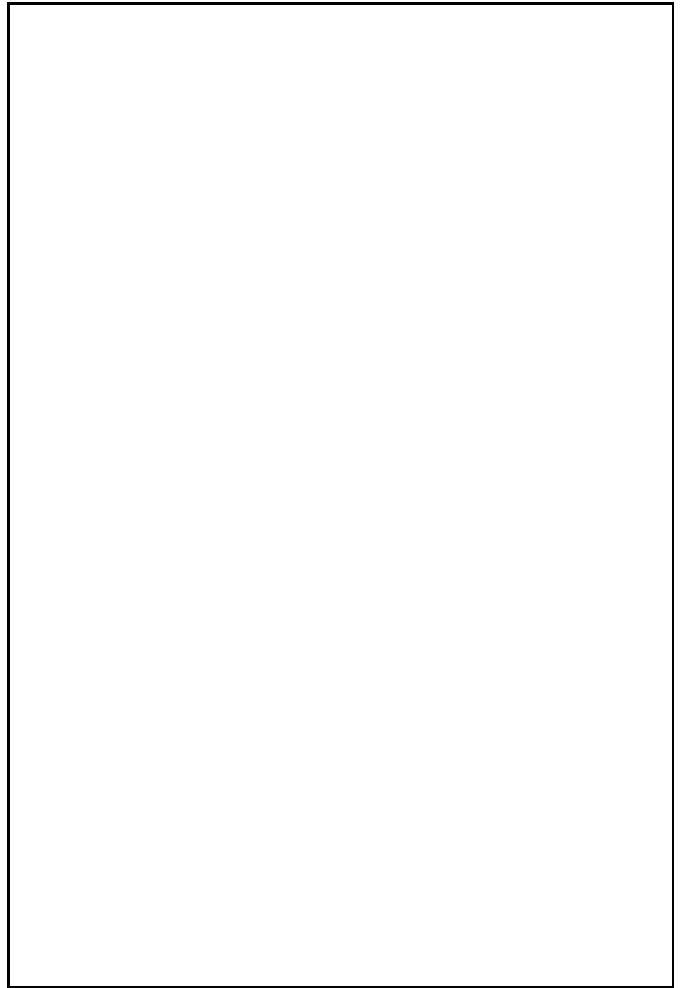


**Fig. 7.** Distributions of magnetic intensity and vectors in a bar perturbation (model  $A4$ ) at  $t = 1.1 \cdot 10^8$  yrs (a) and  $t = 2.2 \cdot 10^8$  yrs (b)

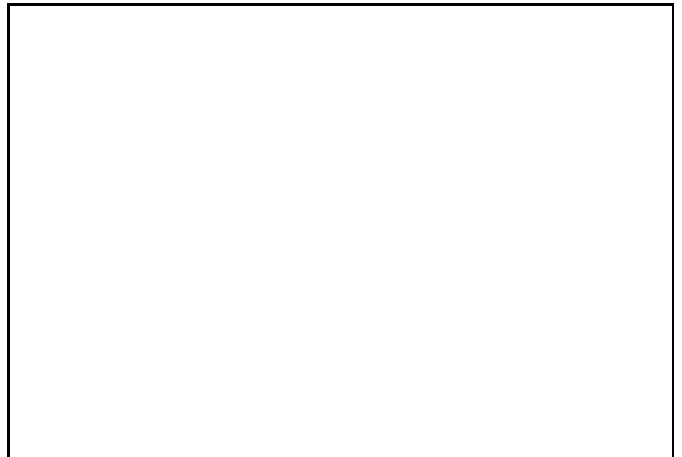


**Fig. 8.** Time evolution of magnetic energy density  $\epsilon$  normalized to the initial energy density  $\epsilon_0$  for the models  $Bi$ . Circ, bar, p20 and p10 denote the velocity field structures: circular, with bar perturbation, with the pitch angle of  $20^\circ$  and  $10^\circ$ , respectively

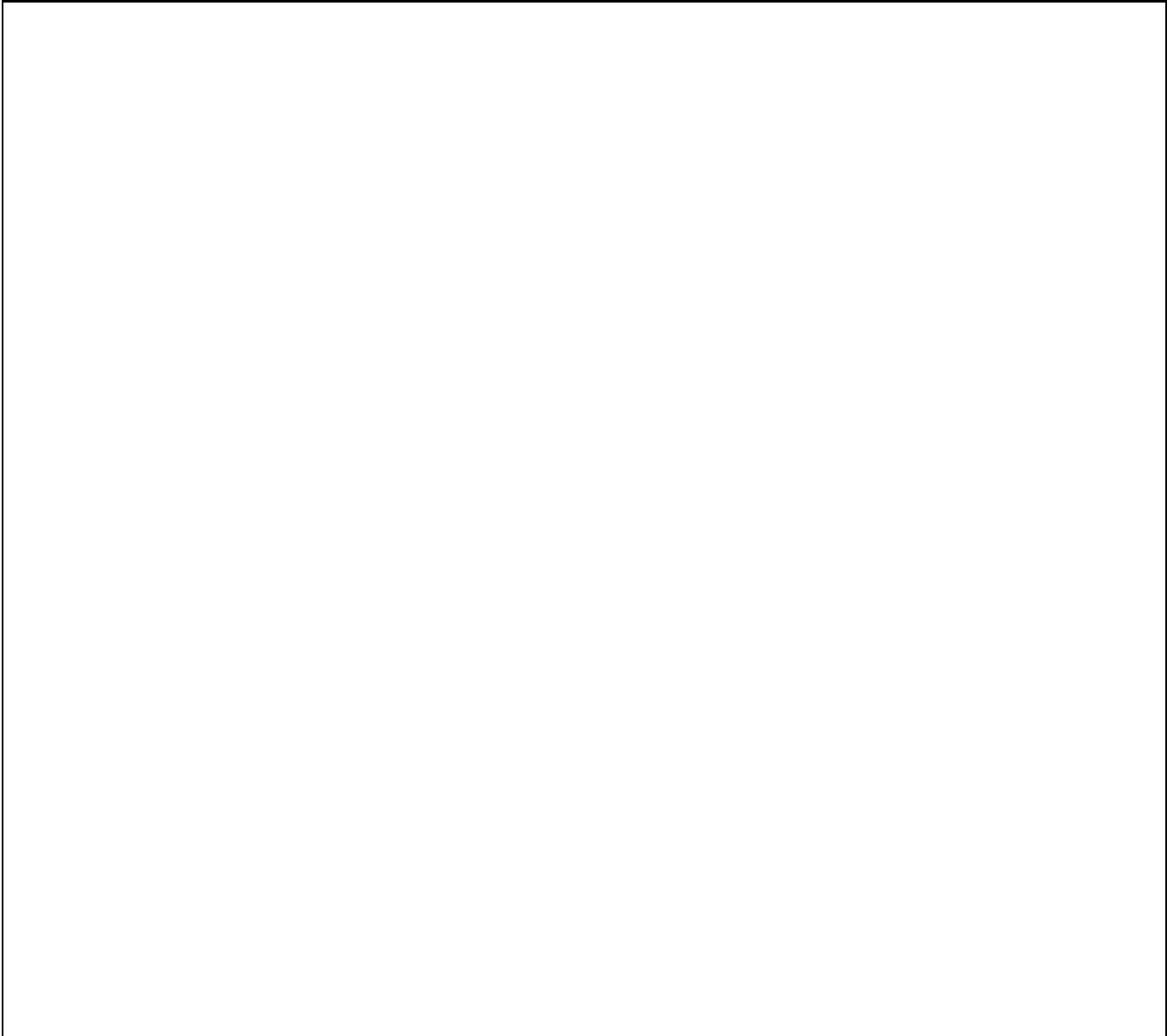


**Fig. 9.** Distributions of magnetic vectors for the model *B7* at 4 evolutionary epochs

merical simulations. First, to obtain the realistic velocity fields for calculations of magnetic fields, the hydrodynamical simulations using SPH scheme have been performed for three potential disturbances in an axisymmetric disk: tightly wound spiral with pitch angle  $\psi$  of  $10^\circ$ , open spiral with  $\psi = 20^\circ$  and bar perturbation. Then, the resultant velocity fields of gas at  $\sim 1.6 \cdot 10^8$  yrs have been used to simulate the evolution of large-scale galactic magnetic fields. Our calculations of magnetic fields are devoted to a disk structure which is well established observationally and theoretically: some other effects such as vertical gas flows are neglected because these are tediously increasing parameters for models. Two basic configurations for the initial magnetic field have been chosen: axisymmetric

(Table 1, *Ai*) and uniform (parallel to the Y axis) (Table 1, *Bi*). The adopted field configurations are enough to demonstrate the net effects of non-axisymmetric flow perturbations on magnetic field structure.

#### 4.1. Magnetic field structure

The robust conclusion from our simulations is that the magnetic field follows closely the interstellar gas motions;

The comparison between magnetic energy and gas density in the case of initially ring magnetic field (*Ai*) shows that the maxima of magnetic energy coincide with those of gas density (Figs. 3, 4, and 6 a and b), and this is also the case for initially uniform field. Both maxima are lo-

cating slightly outside the minima of spiral potential (i.e. down-stream side) within the corotation radius of 9.1 kpc, being the characteristic non-linear response of interstellar gas (if we consider the effects of magnetic pressure consistently, the region of density maxima can be broadened, see e.g. Tubbs 1980).

The pitch angle distributions of both velocity and magnetic fields also indicate the tight correlation between the interstellar gas motion and magnetic-field structure (Fig. 5a, b and c; Fig 6c and d): both distributions of pitch angles are very similar even for the longest evolutionary time. This suggests that the characteristic gas motions involved in a non-axisymmetric disk are dominant enough to organize the field structure even in the presence of turbulent dissipation. The actual spatial variation of field lines of force is summarized as follows: In front of the spiral arm (i.e. upper-stream side), the orientation of magnetic field lines is slightly deviating from the arm, with the absolute value of pitch angle  $\psi$  being small or positive  $\psi$  (i.e. more leading sense than the trailing spiral arm itself). In the arm, the field lines are well aligned with the arm, i.e. the absolute value of  $\psi$  is maximum with the negative sign. Then, outside the arm, the orientation of field lines is changing gradually from the trailing sense in the arm to the leading sense as the gas stream leaves the arm, so that the field crosses with the next arm again with a finite angle. Thus, the variation of the magnetic pitch angles with azimuth is doubly-periodical, and the properties of the pitch-angle variation are essentially in agreement with the observational results for NGC6964 (Ehle & Beck 1993), M51 (Neininger 1992), M83 (Neininger et al. 1991), and M81 (M.Krause, private communication). We remark that the definition of pitch angles by radio observers is different from the usual one, and thus one should be careful when saying the *sign* of pitch angles. Also, our estimate of the field orientation does not include some observational effects such as the beam smoothing, Faraday rotation and the effects of small-scale turbulent fields, so that the observed distribution of the field lines obtained above may be somewhat different but the general properties of field structure across the arm may be unchanged.

We have clarified that the actual structure of magnetic field is well correlated with the optical structure of a galactic disk as radio observations have revealed. We are thus puzzled how other approaches based on conventional  $\alpha\omega$ -dynamos with only an axisymmetric disk can explain such universal correlation without relying on spiral-arm disturbance.

#### 4.2. Time evolution of magnetic field energy

All of our simulated models result in the decay of magnetic energy density in the absence of field generation mechanisms. In the cases of initially ring fields (*Ai*), the magnetic energy density,  $\epsilon$ , simply decreases with the evolutionary time due to the weakness of the coupling be-

tween convectional motion of gas and magnetic fields,  $|\mathbf{v} \times \mathbf{B}| \ll 1$ . As mentioned before, each model suggests the amplification of magnetic field in the arm due to compressional and additional shearing motions of gas induced by the arm; the strongest amplification is obtained for the spiral potential when the pitch angle  $\psi$  of  $20^\circ$  (*A3*). On the other hand, the experiments *Bi* have resulted in the wound magnetic-field configurations causing the initial growth of the magnetic energy density  $\epsilon$  in the first  $10^8$  yrs of evolution (Fig. 8). The fast increase of  $\epsilon$  is followed by quick decaying of its value due to the winding of magnetic lines and the resultant stimulated effects of diffusion. The higher non-axisymmetric gas flow causes the lower growth of the magnetic energy density because of the stronger reconnection of the magnetic field lines. In two given cases (*B5* and *B7*), the longer sustaining of  $\epsilon$  is observed: in the case *B5* with the diffusion coefficient variable in the galactic plane and in the experiment *B7* with the high value of the magnetic Reynolds number of 430. The case *B5* has the smaller average value of  $\eta$  and higher  $R_m$  (178) than others, so the slower decrease of  $\epsilon$  is understandable.

The anti-dynamo theorem says that any two-dimensional flows result in the decay of magnetic fields (e.g. Zeldovich et al. 1983). This is due to the absence of the coupling between the field components along the plane of flows and the perpendicular field component. No coupling is eventually followed by the catastrophic reduction of the characteristic scale of magnetic fields, and thus the dissipation. As is well known, the so-called dynamo cycle relying on helical motion of turbulence can introduce the coupling among three components of magnetic fields. A disadvantage in galactic dynamo theory is that it is not obvious concerning the actual existence of helical interstellar turbulence from both theory and observation (*cf.* Ferrière 1992; Hanasz & Lesch 1993; Kaisig et al. 1993). Spencer & Cram (1992) have made the important progress by proposing a new field-generation mechanism relying on global galactic winds. This approach is however also subject to the uncertainty as to whether such preferential winds can be realized in an actual galaxy. It is also worthwhile to note that their model is based on an axisymmetric disk, and thus suggesting the generation of non-axisymmetric magnetic fields in order not to break the anti-dynamo theorem. The emergence of non-axisymmetric fields will give rise to the existence of non-axisymmetric coupling terms between velocity and magnetic fields, which will eventually affect the basic mechanism of field generation from an axisymmetric disk. The general analysis of such a system is now underway (Spencer, private communication). On the other hand, observations of edge-on galaxies suggest the mass outflow from a disk to a halo (e.g. Bloemen 1991), though it is not clear as to whether such vertical flow is occurring steadily or intermittently.

Therefore, it is necessary to consider the general problem of magnetic-field evolution containing the realistic ver-

tical gas flow and the non-axisymmetric velocity disturbance. If the condition for a dynamo is fulfilled in such a system, the growth of magnetic fields can be very fast when the efficient amplification due to non-axisymmetric disturbance, e.g. the wave coupling between density and magnetic waves, is considered (Chiba & Lesch 1994), which we have neglected here by suppressing the propagation effect of spiral arms with azimuth in the simulations.

#### 4.3. Effects of azimuthally varied $\eta$

In the present numerical experiments, we have explored the possibility that the dissipation effects for magnetic fields are spatially varied in a galactic plane. Usually the coefficient  $\eta$  of turbulent diffusion has been assumed to be uniform in a plane for galactic dynamos. Ko & Parker (1989) have examined the time-dependent dynamo on the assumption of spatial variability in dynamo efficiency driven by young OB stars and supernovae in spiral arms. The energy transformation from stellar winds and explosions to interstellar medium gives rise to high velocity dispersion of turbulence, thereby enhancing the dissipation of magnetic fields. Mestel & Subramanian (1991) considered the enhancement of helical turbulence ( $\alpha$ -effects) in spiral arms. Though the exact expression for  $\eta(\varphi)$  is unknown, it is interesting to see how the effect is non-trivial for magnetic-field evolution.

The model with the diffusion coefficient variable in the galactic plane (A2) has resulted in higher amplification of magnetic intensity in the spiral arms than in the case for  $\eta$  constant in the plane (A1). This is well explained by the transport of magnetic flux from the region where diffusion is high (in our case, the minima of potential perturbation) to the region where diffusion is weak. The gas streaming motion across the arm prohibits the leakage of magnetic flux towards the upper-stream side, so the magnetic intensity is magnified at the down-stream side of spiral arms. If we consider the generation of small-scale magnetic fields from such intense turbulence, the total strength of magnetic fields can be the highest in the arm regions. Furthermore, the contrast in magnetic pitch angles is also magnified in this case (Fig. 5b), probably due to the higher coupling between velocity and magnetic fields in the inter-arm regions where  $\eta$  is assumed to be small.

One more noticeable point for the case of spatially varied  $\eta$  is that the decay of magnetic field energy is made much slower (Fig. 8). Therefore, more realistic may be the rather slow dissipation of large-scale magnetic fields compared to the usually voiced value of dissipation time scale of  $\sim 10^8$  yr. Further studies about this point are necessary before drawing such conclusions.

*Acknowledgements.* We are grateful to Harald Lesch, Marek Urbanik, Steve Spencer, Rainer Beck, and Elly Berkhuijsen for their helpful comments and discussions. KO wishes also to express her gratitude to Zbigniew Kosma and Marian Soida for their valuable advice during this work. Calculations have

been supported by the Forschungszentrum Jülich GmbH. KO thanks the hospitality of Max-Planck-Institute in Bonn, and MC thanks the Alexander von Humboldt Foundation for support. This work was partly supported by the grant from Polish Committee for Scientific Research (KBN), grant no. PB/0628/P3/93/04.

## References

- Beck, R., 1993, in *The Cosmic Dynamo*, eds. F.Krause, K-H Rädler, G.Rüdiger, IAU Symp. 157, Kluwer, Dordrecht, p.283
- Benz, W., 1990, in *Numerical Modeling of Nonlinear Stellar Pulsation: Problems and Prospects*, ed. J.R.Buchler, NATO ASI series, Kluwer, Dordrecht, p.269
- Binney, J., Tremaine, S., 1987, *Galactic Dynamics*, Princeton University Press, Princeton
- Bloemen, H. (ed) 1991, *The Interstellar Disk-Halo Connection in Galaxies*, IAU Symp. 144, Kluwer, Dordrecht
- Camenzind, M., Lesch, H., 1994, *A&A*, 284, 411
- Chiba, M., Lesch, H., 1994, *A&A*, 284, 731
- Ehle, M., Beck, R., 1993, *A&A*, 273, 45
- Elstner, D., Meinel, R., Rüdiger, G., 1990, *Geophys. Astrophys. Fluid Dyn.*, 50, 85
- Evans, C.R., Hawley, J.F., 1988, *ApJ*, 332, 659
- Ferrière, K., 1992, *ApJ*, 389, 286
- Gingold, R.A., Monaghan, J.J., 1977, *MN*, 181, 375
- Habe, A., Uchida, Y., Ikeuchi, S., Pudritz, R.E., 1991, *PASJ*, 43, 703
- Hanasz, M., Lesch, H., 1993, *A&A*, 278, 561
- Hernquist, L., Katz, N., 1989, *ApJS*, 70, 419
- Horellou, C., Beck, R., Berkhuijsen, E.H., Krause, M., Klein, U., 1993, *A&A*, 265, 417
- Johns, T.C., Nelson, A.T., 1986, *MN*, 220, 165
- Kaisig, M., Rüdiger, G., Yorke, H.W., 1993, *A&A*, 274, 757
- Kichatinov, L.L., Rüdiger, G., 1992, *A&A*, 260, 494
- Ko, Parker, E.N., 1989, *ApJ*, 341, 828
- Krause, F., Rädler, K-H, Rüdiger, G., (eds) 1993, *The Cosmic Dynamo*, IAU Symp. 157, Kluwer, Dordrecht
- Kronberg, P.P., Perry, J.J., Zukowski, E.L.H., 1992, *ApJ*, 387, 528
- Kronberg, P.P., 1994, *Rep.Prog.Phys.*, 325
- Lesch, H., Chiba, M., 1994, *A&A*, in press
- Lesch, H., 1993, in *The Cosmic Dynamo*, eds. F.Krause, K-H Rädler, G.Rüdiger, IAU Symp. 157, Kluwer, Dordrecht, p.395
- Lucy, L., 1977, *AJ*, 82, 1013
- Matsuda, T., Isaka, H., 1980, *Prog. theor. Phys.*, 64, 1265
- Mestel, L., Subramanian, K., 1991, *MN*, 248, 677
- Monaghan, J.J., 1992, *ARA&A*, 30, 543
- Monaghan, J.J., Lattanzio, J.C., 1985, *A&A*, 149, 135
- Neininger, N., Klein, U., Beck, R., Wielebinski, R. 1991, *Nat.*, 352, 781
- Neininger, N., 1992, *A&A*, 263, 30
- Neininger, N., Beck, R., Sukumar, S., Allen, R.J., 1993, *A&A*, 274, 687
- Panesar, J.S., Nelson, A.H., 1992, *A&A*, 264, 77
- Rüdiger, G., Elstner, D., Schultz, M., 1993, in *The Cosmic Dynamo*, eds. F.Krause, K-H Rädler, G.Rüdiger, IAU Symp. 157, Kluwer, Dordrecht, p.321

- Schmidt-Voigt, M., 1987, in *Interstellar Magnetic Fields*, eds.  
R. Beck, R. Gräve, Springer, Berlin, p.251
- Schmidt-Voigt, M., 1989, *A&A*, 210, 433
- Spencer, S.J., Cram, L.E., 1992, *ApJ*, 400, 484
- Toomre, A., 1963, *ApJ*, 138, 385
- Tubbs, A.D., 1980, *ApJ*, 239, 882
- Wolfe, A.M., Lanzetta, K.M., Oren, A.L., 1992, *ApJ*, 388, 17
- Zeldovich, Ya.B., Ruzmaikin, A.A., Sokoloff, D.D., 1983, *Magnetic Fields in Astrophysics*, Gordon and Breach